Advances in Materials
2025; 14(1): 30-35
http://www.sciencepublishinggroup.com/j/am
doi: 10.11648/j.am.20251401.14
ISSN: 2327-2503 (Print); ISSN: 2327-252X (Online)

Competing Kondo Singlet and Magnetic Order Insulator in Graphene Lattices: A Variational Cluster Approximation Approach

Jean Paul Latyr Faye*, Oumar Ndiaye, Allé Dioum, Alassane Traoré

Department of Physics, Faculty of Science and Technology, Cheikh Anta Diop University, Dakar-Fann, Dakar, Senegal

Email address:

jeanpaullatyr.faye@ucad.edu.sn (Jean Paul Latyr Faye)
*Corresponding author

To cite this article:

Jean Paul Latyr Faye, Oumar Ndiaye, Allé Dioum, Alassane Traoré. (2025). Competing Kondo Singlet and Magnetic Order Insulator in Graphene Lattices: A Variational Cluster Approximation Approach. *Advances in Materials, 14*(1), 30-35.
https://doi.org/10.11648/j.am.20251401.14

Received: 24 February 2025; **Accepted:** 17 March 2025; **Published:** 25 March 2025

Abstract: Strongly correlated electron systems, where localized magnetic moments interact with conduction electrons, continue to challenge our understanding of quantum phases. In particular, the competition between the Kondo effect-which promotes the formation of singlet states via the screening of localized spins-and magnetic ordering driven by the Ruderman-Kittel-Kasuya-Yosida (RKKY) interaction, plays a crucial role in defining the electronic properties of materials such as graphene and other honeycomb lattice systems. In this work, we investigate the interplay between these competing mechanisms using a Kondo-Hubbard model on the hexagonal lattice. Our model incorporates key interactions including the Kondo coupling $J_\perp$ between conduction electrons and localized spins, the Heisenberg exchange J_H between localized moments, the onsite Coulomb repulsion U for conduction electrons, and a second nearest-neighbor hopping term t'. The study is conducted at half-filling, where each lattice site hosts one electron on average, and the system is analyzed via the variational cluster approximation (VCA) combined with an exact diagonalization solver at zero temperature. Our analysis focuses on mapping the phase diagrams in different parameter spaces, particularly the $(J_H, J_\perp)$ and $(J_\perp, UJ_\perp)$ planes. We find that the antiferromagnetic phase is favored at smaller $J_\perp$ and larger J_H, while an increase in $J_\perp$ stabilizes the Kondo singlet phase. The transition between these phases occurs smoothly, indicating a second-order phase transition. Additionally, the inclusion of the hopping term t' is shown to enhance the stability of the Kondo singlet phase. Overall, our results provide new insights into the delicate balance between magnetic order and Kondo singlet formation in low-dimensional correlated systems, potentially guiding future experimental and theoretical investigations in graphene-based materials and related compounds.

Keywords: Kondo Lattice, Graphene, Variational Cluster Approximation, Magnetic Order, Strong Correlations

1. Introduction

Quantum systems featuring both itinerant electrons and localized moments continue to draw significant attention in modern condensed matter physics due to their intriguing behaviors. These include the formation of heavy quasi-particles in heavy electron compounds containing rare earth elements [1], the discovery of unconventional superconductivity [2] first observed in UBe_{13} [3], and non-Fermi liquid behavior [4]. Two key interactions between itinerant and localized moments are the Kondo effect [5] and the Ruderman-Kittel-Kasuya-Yosida (RKKY) interaction [6].

On one hand, the Kondo effect results from the coupling between conduction electrons and localized magnetic moments, which tends to form a singlet state. In this scenario, a localized spin interacts with the surrounding sea of conduction electrons, and through a process of repeated scattering, the magnetic moment is screened by the electrons. This leads to the formation of a Kondo singlet state. As a result, the system tends towards a non-magnetic, Fermi-liquid-like ground state at low temperatures.

On the other hand, the RKKY interaction arises from

indirect exchange interactions between localized magnetic moments, mediated by the conduction electrons. In contrast to the Kondo effect, the RKKY interaction favors the establishment of a magnetically ordered state. The competition between the Kondo singlet formation and RKKY-induced magnetic ordering creates balance. In certain materials, the balance can be tuned by changing external parameters such as pressure, magnetic field, or doping, leading to a quantum critical point.

Two-dimensional magnetic materials have attracted substantial interest in recent years due to their potential applications in spintronic devices, the presence of quantum spin liquid phases, which have potential uses in topological quantum computing. The physics of the Kondo lattice model on non-frustrated lattices, such as square lattices, has been extensively studied [7]. Recently, it has also been explored in frustrated lattices, such as the triangular lattice [8].

The honeycomb lattice systems have been extensively explored, particularly in correlated electron systems like graphene [9] and silicene [10], where numerous exotic phenomena have been discovered both theoretically and experimentally. Although the honeycomb lattice is bipartite, it has the smallest possible coordination number among proper two-dimensional lattices. This distinction allows the honeycomb lattice to exhibit physical phenomena that are fundamentally different from those seen in square lattices. Examples include the spin-liquid phase and quantum criticality in the Hubbard model [11], as well as the topological Mott insulator in the extended Hubbard model [12]. The coupling of conduction electrons to local magnetic moments has been achieved in graphene, leading to the observation of the Kondo effect associated with point defects [13]. The formation of the Kondo singlet causes the system to transition from a semimetal to a Fermi liquid with a finite density of states [14]. The Kondo effect in honeycomb lattice could be realized in transition metal oxides such as $(Bi_3Mn_4O_{12})NO_3$ and Li_2MnO_3, with Mn ions forming the honeycomb lattice [15]. The Kondo effect can also be realized in ultracold atom [16]. However, the interaction between conduction electrons and the densely localized spins on the honeycomb lattice, which can be described by the Hubbard-Kondo lattice model, remains a largely unresolved issue.

This papers explores the interplay between the Kondo effect and magnetic ordering induced by RKKY interaction on the honeycomb lattice model, employing the variational cluster approximation with an exact diagonalization solver at zero temperature. The infinite lattice is divided into identical 6-site clusters, that together tile the entire lattice. Two localized spins, interacting via the Heisenberg interaction (J_H), are introduced, which interact with the conduction electrons through the coupling constant $J_\perp$. At half-filling, we obtain two phase diagrams. In the $(J_H, J_\perp)$ plane, the antiferromagnetic phase is favored for small J_H and moderate $J_\perp$, while the Kondo singlet is favored at larger values of $J_\perp$. In the $(J_\perp, UJ_\perp)$ plane, the antiferromagnetic phase dominates for small to moderate values of $J_\perp$ and $UJ_\perp$, while the Kondo singlet phase appears elsewhere.

The paper is organized as follows: Section 2 provides a description of the model Hamiltonian and the variational cluster approximation method. Section 3 discusses the results, and we conclude in Section 4.

2. Model and Method

2.1. Model Hamiltonian

The model Hamiltonian consists of two terms: the Kondo Hamiltonian $\mathrm{H_K}$ and the Hubbard Hamiltonian $\mathrm{H_H}$:

$$\mathrm{H} = \mathrm{H_K} + \mathrm{H_H} \tag{1}$$

The Kondo Hamiltonian can be written as follows:

$$\begin{aligned} \mathrm{H}_K &= -t \sum_{\mathbf{r}\in\mathbf{A},\sigma,\mathbf{j}} \left(c^\dagger_{\mathbf{r},\sigma} c_{\mathbf{r}+\mathbf{e_j},\sigma} + \mathrm{H.c.}\right) + J_\perp \sum_{\mathbf{r}\in\mathbf{A}} \mathbf{s_r}\cdot\mathbf{s}^f_u + J_\perp \sum_{\mathbf{r}\in\mathbf{B}} \mathbf{s_r}\cdot\mathbf{s}^f_d - t' \sum_{\mathbf{r}\in\mathbf{A},\sigma,\mathbf{j}} \left(c^\dagger_{\mathbf{r}\sigma} c_{\mathbf{r}\pm\mathbf{2e_j}\sigma} + \mathrm{H.c.}\right) \\ &\quad + J_\mathrm{H}\, \mathbf{s}^f_u \cdot \mathbf{s}^f_d + \mu \sum_{\mathbf{r}\in\mathbf{A},\mathbf{B}} n_\mathbf{r}. \end{aligned} \tag{2}$$

In addition to the Kondo term characterized by $J_\perp$, H_K incorporates the first and second-nearest neighbor hopping terms t and t'. To take into account spin interactions between the two localized electrons, labeled with indices u and d, we introduce the Heisenberg interaction term, defined by the coupling constant J_H. $J_\perp$, which we will assume to have an antiferromagnetic coupling, couples the conduction spins, at site $\mathbf{r}$, $\mathbf{s_r} = \frac{1}{2} c^\dagger_{\mathbf{r}\sigma} \tau_{\sigma,\sigma'} c_{\mathbf{r}\sigma'}$ and the localized spins $\mathbf{s}^f_{u(d)} = \frac{1}{2} f^\dagger_{u(d)\ \sigma} \tau_{\sigma,\sigma'} f_{u(d)\ \sigma'}$, where $\tau_{\sigma,\sigma'}$ are the Pauli matrices; $c_{\mathbf{r}\sigma}$ ($c^\dagger_{\mathbf{r}\sigma}$) annihilate (create) a conduction electron at site $\mathbf{r}$ with spin orientation σ, while $f_{u(d)\sigma}$ ($f^\dagger_{u(d)\sigma}$) annihilate (create) a localized electron at site u or d with spin orientation σ.

The Hubbard Hamiltonian writes:

$$\mathrm{H}_H = U \sum_{\mathbf{r}\in\mathbf{A},\mathbf{B}} n_{\mathbf{r}\uparrow} n_{\mathbf{r}\downarrow} + U_f \left(n^f_{u\uparrow} n^f_{u\downarrow} + n^f_{d\uparrow} n^f_{d\downarrow}\right) \tag{3}$$

Here, U is the one-site Coulomb interaction for conduction electrons, $U_f = 20t$ for itinerant electrons, and $n_{\mathbf{r}\sigma} = c^\dagger_{\mathbf{r}\sigma} c_{\mathbf{r}\sigma}$ denotes the electron density operator, which determines the number of electrons at site $\mathbf{r}$ with spin orientation σ.

2.2. Variational Cluster Approximation Method

The model described by Eq. (1) incorporates the interaction term through the one-site Coulomb interaction U. Addressing

U necessitates employing a method capable of handling it exactly, at least with a restricted space. In this context, we utilize the Variational Cluster Approximation (VCA) with an exact diagonalization solver at zero temperature [17].

VCA is a method that divides the lattice into small identical clusters, each described by the Hamiltonian H', referred to as the reference Hamiltonian. The Hamiltonian H' is derived from the lattice Hamiltonian H by setting to zero the off-diagonal elements of the hopping matrix, but conserving exactly the interaction term. The hopping terms connecting the clusters are treated using perturbation theory. Thus, VCA can be regarded as an extension of the Cluster Perturbation Theory (CPT) [18], which is rooted in Potthoff's self-energy functional approach [19].

To study broken symmetries of different phases and their competitions, a Weiss field for each phase should be added to H'. It is also possible to add to H' any single-body term, which can be varied as a model parameter.

VCA has been shown to perform well when studying the competition between different broken symmetries such as superconductivity and magnetism in strongly correlated systems such as cuprates [20].

In Figure 1, we present the tiled hexagonal lattice featuring a 6-site cluster with the impurity positioned at its center. It is worth noting that, in the VCA, the cluster size is constrained due to the requirement for exact diagonalization to solve the cluster accurately.

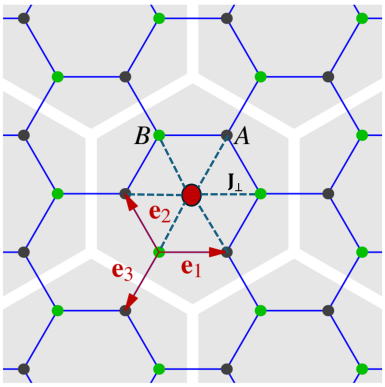

Figure 1. *(Color online) Tiling of the hexagonal lattice by 6-site clusters (gray shading) used in VCA. The A and B sublattices are indicated, as well as the three elementary vectors* $\mathbf{e}_{1,2,3}$*. The red dots represent the impurities.*

To find the optimal one-body part of H', that is the solution, we use the variational principle, where the electron self-energy Σ associated with H' is the variational parameter. The Potthoff self-energy functional can be written as: [19]:

$$\begin{aligned}\Omega[\Sigma(\lambda)] &= \Omega'[\Sigma(\lambda)] + \mathrm{Tr}\ln[-(\mathbf{G}_0^{-1} - \Sigma(\lambda))^{-1}] \\ &- \mathrm{Tr}\ln(-\mathbf{G}'(\lambda)) \end{aligned} \quad (4)$$

In Eq. (4), $\mathbf{G}'$ and $\mathbf{G}_0$ are respectively the physical and the non-interacting Green function of the cluster and the lattice; and all the parameters that define H' are incorporated in λ. The trace, Tr, is a functional trace in the sense that it includes a sum of frequencies, momenta, and bands. The grand potential of the cluster is denoted by Ω'. It will correspond to the ground state energy of the cluster when the electron self-energy Σ is at its optimal value. In order to obtain the values of $\mathbf{G}'(\omega)$ and Ω', we use numerical techniques, such as the Lanczos method. Within the restricted space of the self-energies $\Sigma(\lambda)$, we exactly compute the Potthoff functional $\Omega[\Sigma(\lambda)]$ that are the physical self-energies of H'. We use the Newton-Raphson optimization method to find the stationary value of $\Omega(\lambda)$ as follows:

$$\frac{\partial\Omega(\lambda)}{\partial\lambda} = 0 \quad (5)$$

The stationary value of $\Omega(\lambda)$ leads to the best value of Σ that we combine with $\mathbf{G}_0$ to construct an approximate $\mathbf{G}$ for the original lattice Hamiltonian H. Finally, for $\mathbf{G}$, we compute the expectation values of all the one-body operators added to H'. In this work, the expectation value of the antiferromagnetism operator $\hat{\mathbf{M}}$, in Eq. (6), is computed leading to its order parameter, denoted AFM.

Eq. (5) can yield two stationary solutions: one corresponding to a zero Weiss field and the other to a finite Weiss field. The solution with zero Weiss field represents the normal state, while the solution with a non-zero Weiss field describes the broken symmetry state, specifically antiferromagnetism in this context. Between those possibilities, the true solution corresponds to the one with the lowest grand potential Ω.

In summary, the VCA implementation involves dividing the lattice into manageable clusters solved by ED and then reintroducing inter-cluster correlations perturbatively. The choice of cluster size and boundary conditions are critical to the quality of the approximation, and additional variational parameters can be used to correct for boundary effects. The limitations of ED, notably the exponential scaling of the Hilbert space and finite-size effects, restrict the size of clusters that can be used, which in turn limits the extent to which non-local correlations are captured. This careful balance between computational feasibility and physical accuracy is central to the practical application of VCA in studying strongly correlated systems.

3. Results and Discussions

To capture the antiferromagnetism, we add in Hamiltonian (1) the operator:

$$\mathbf{A\hat{F}M} = \mathrm{h_{AF}}\left(\sum_{\mathbf{r}\in\mathbf{A}}(\mathrm{n}_{\mathbf{r}\uparrow} - \mathrm{n}_{\mathbf{r}\downarrow}) - \sum_{\mathbf{r}\in\mathbf{B}}(\mathrm{n}_{\mathbf{r}\uparrow} - \mathrm{n}_{\mathbf{r}\downarrow})\right), \quad (6)$$

based on the difference in spin density between two sublattices of the original system where h_{AF} represents the Weiss field.

In Figure 2, we present the antiferromagnetic order parameter (AFM), the expectation value of $\hat{\mathbf{M}}$, as a function of $\mathrm{J}_\perp$ for different $\mathrm{J_H}$, at $\mathrm{U} = 5\mathrm{t}$. All the results are obtained

at half-filling ($\mu = U/2$) where each site in the cluster has one electron on average and are given in units of t.

To avoid double occupancy of localized electron sites, we set $U_f = 20t$, larger than the other model parameters. The system is then studied for two different cases of $\mathrm{t}' = 0$ and $\mathrm{t}' = -0.1\mathrm{t}$ for different values of $\mathrm{J_H}$, represented in the top and lower panels, respectively.

The results for $\mathrm{t}' = 0$ reveal how the critical values of $\mathrm{J}_\perp$ increase as $\mathrm{J_H}$ are enhanced. Thus, for larger values of $\mathrm{J_H}$, higher values of $\mathrm{J}_\perp$ are required to transition the system from the antiferromagnetic phase to the Kondo singlet phase.

The lower panel, $\mathrm{t}' = -0.1\mathrm{t}$, shows the effect of t', where the increase in the critical value of $\mathrm{J}_\perp$ with increasing $\mathrm{J_H}$ is less pronounced compared to the top panel. This observation can be explained by the fact that t' tends to promote the formation of the Kondo singlet phase, as it creates a favorable environment for the coupling between conduction and localized electrons. On the other hand, $\mathrm{J_H}$ supports the formation of the antiferromagnetic phase, as it couples the localized spins in such a way that they tend to align antiparallel to each other, leading to a non-zero magnetization.

We observe that as $\mathrm{J}_\perp$ increases, the antiferromagnetic order parameter gradually decreases. At a certain critical value of $\mathrm{J}_\perp$, the order parameter vanishes completely, signaling the transition from the antiferromagnetic phase to the Kondo singlet phase. This smooth decrease of the antiferromagnetic order parameter as a function of $\mathrm{J}_\perp$ is consistent with a second-order phase transition, where the transition between the two phases occurs without any discontinuous jump in the order parameter.

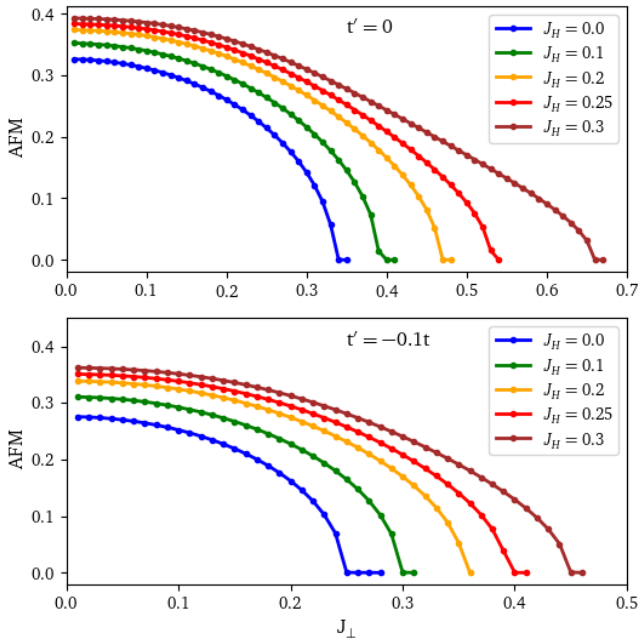

Figure 2. *AFM order parameter as a function of* $\mathrm{J}_\perp$ *for different values of* $\mathrm{J_H}$ *at* $\mathrm{U} = 5\mathrm{t}$. *The top panel displays results for* $\mathrm{t}' = 0$, *while the bottom panel shows the case for* $\mathrm{t}' = -0.1\mathrm{t}$. *A second-order phase transition is evident from the smooth disappearance of the AFM.*

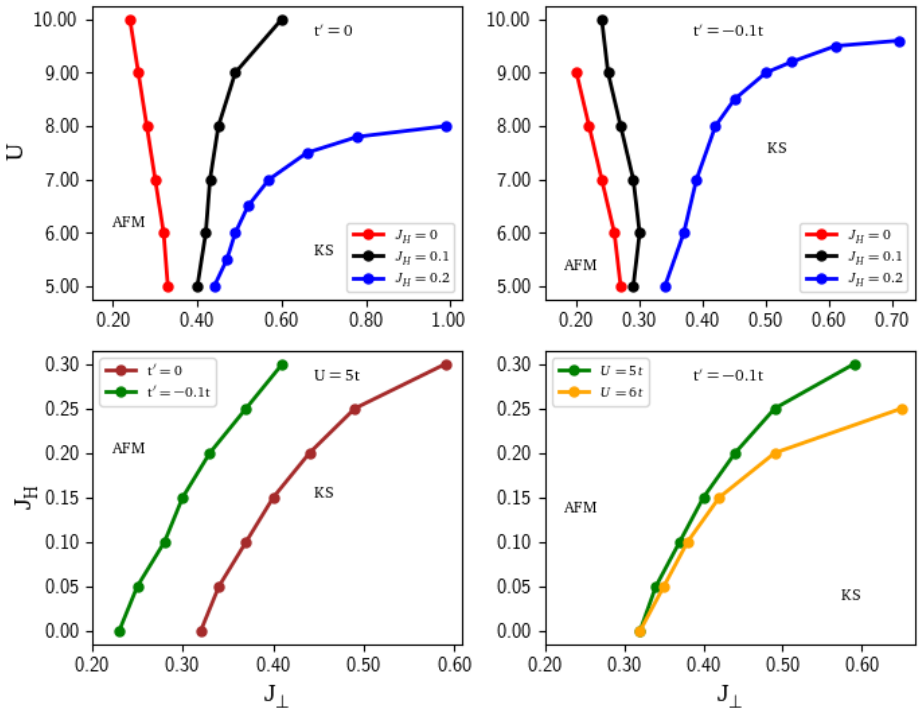

Figure 3. *Phase diagrams: (i) In the* $\mathrm{U}, \mathrm{J}_\perp$ *plane for (a)* ($\mathrm{J_H} = 0$) *and (b)* $\mathrm{J_H} = 0.2\mathrm{t}$, *with (top left)* $\mathrm{t}' = 0$ *and (top right)* $\mathrm{t}' = -0.1\mathrm{t}$. *(ii) In the* $(\mathrm{J_H}, \mathrm{J}_\perp)$ *plane: (bottom left) for* $\mathrm{t}' = 0$ *and* $\mathrm{t}' = -0.1\mathrm{t}$ *at* $\mathrm{U} = 5\mathrm{t}$, *and (bottom right) for* $\mathrm{U} = 5\mathrm{t}$ *and* $\mathrm{U} = 6\mathrm{t}$ *at* $\mathrm{t}' = -0.1\mathrm{t}$. *The Kondo singlet (KS) and the antiferromagnetism (AFM) phases are indicated.*

Figure 3 presents a comprehensive set of phase diagrams, exploring various parameter combinations that govern the system's behavior. These diagrams are organized into two primary sections, providing insights into the interplay between different interactions: the top panels show the phase diagrams in the $(\mathrm{J}_\perp, U)$ plane, while the bottom panels examine the phase diagrams in the $(\mathrm{J}_\perp, \mathrm{J_H})$ plane.

Top panel: phase diagrams in the $(\mathrm{J}_\perp, U)$ plane − The left panel, corresponding to $\mathrm{t}' = 0$, reveals significant insights into the system's phase behavior as a function of U. We observe that increasing U does not lead to the stabilization of the AFM phase, which is a typical characteristic of many strongly correlated systems. U tends to localize the electrons, promoting the formation of Kondo singlets, which dominate over the AFM phase.

The inclusion of $\mathrm{J_H}$ changes the dynamics significantly. Increasing $\mathrm{J_H}$ expands the region of the AFM phase and simultaneously reduces the Kondo singlet phase. This shows that $\mathrm{J_H}$ and $\mathrm{J}_\perp$ have opposing effects on these two phases. While $\mathrm{J_H}$ promotes antiferromagnetism, $\mathrm{J}_\perp$ tends to favor the Kondo singlet phase, and their combined effects govern the overall phase structure.

The right panel of the top row corresponds to $\mathrm{t}' = -0.1t$. We remark that, in the presence of t', a stronger U is required to transition the system from the Kondo singlet phase to the AFM phase.

Bottom panel: phase diagrams in the $(\mathrm{J}_\perp, \mathrm{J_H})$ plane − The left panel explores the phase diagram in the $(\mathrm{J}_\perp, \mathrm{J_H})$ plane for $U = 5t$, and compares the cases for $\mathrm{t}' = 0$ and $\mathrm{t}' = -0.1t$. The results show how the AFM gets more room by pushing the Kondo singlet phase to smaller regions as $\mathrm{J_H}$ increases. In contrast, the presence of t' reduces this effect. When $\mathrm{t}' = -0.1t$, the Kondo singlet phase is more pronounced compared to the case $\mathrm{t}' = 0$.

Bottom right panel: effect of Coulomb interaction on the phase diagram − As U increases, the phase diagram undergoes a transition, with the Kondo singlet phase shrinking and the AFM phase expanding.

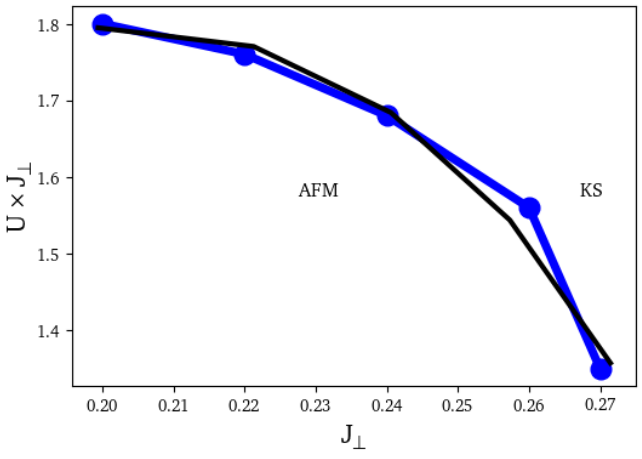

Figure 4. *Phase diagram in the $(\mathrm{J}_\perp, \mathrm{UJ}_\perp)$ plane (blue dotted curve) for $\mathrm{U_f} = 20\mathrm{t}$, $J_H = 0$, and $\mathrm{t}' = -0.1\mathrm{t}$. The fitting to the data lead to $\alpha = 1.0$ and $\beta = 0.30$ in equation (7) represented by the black curve.*

The phase diagram presented in Figure 4, consolidates all critical values of $J_\perp$ obtained for various values of U at $J_H = 0$ and $\mathrm{t}' = -0.1\mathrm{t}$. The obtained phase diagram aligns well with other results from VCA and Monte Carlo simulations. A particularly interesting observation is the behavior of the critical value of U as a function of $J_\perp$. When $J_\perp$ is small, the critical value of U scales inversely with $J_\perp$, i.e., the phase boundary approaches a finite value of the product $UJ_\perp$ as $J_\perp \to 0$. However, despite this trend, at $J_\perp = 0$, the system remains strictly in the AFM phase. Conversely, when $J_\perp$ becomes sufficiently large, the system always transitions into the Kondo singlet phase.

Theoretical insights from the study of Kondo insulators offer a deeper understanding of the critical boundary separating the AFM and Kondo singlet phases. The leading-order behavior of the phase boundary is described by the equation:

$$J_\perp^2 + aJ_\perp^2 U = b \tag{7}$$

where the fitting to the data leads to $a = 1.0$ and $b = 0.3$. This equation implies that the phase boundary has a parabolic shape, which is consistent with the appearance of the phase diagram in Figure 4. This formulation highlights how the Hubbard interaction U enhances the Kondo singlet phase. Specifically, U contributes to the effective coupling in a manner analogous to $J_\perp$, effectively increasing the total interaction strength that stabilizes the Kondo singlet phase.

4. Conclusion

In this work, we investigate the competition between Kondo singlet and magnetic order phases using the Kondo-Hubbard model on the hexagonal lattice. The model includes the local Coulomb interaction U, the Kondo coupling $J_\perp$, and the Heisenberg exchange interaction J_H. An impurity atom is added at the center of each hexagon (cluster) of the lattice. We use Variational Cluster Approximation with exact diagonalization at zero temperature to solve the Hamiltonian of the lattice.

At half-filling, we obtain the phase diagram in the $(J_\perp, UJ_\perp)$ plane, which indicates that the Néel magnetic order phase is dominant at lower and intermediate $J_\perp$ and U, while the Kondo singlet phase gets more room at higher $J_\perp$. We show that the transition from the antiferromagnetic order phase to the Kondo singlet phase is a second-order phase transition.

In the $(J_\perp, J_H)$ plane, we find that the Heisenberg exchange interaction J_H effectively pushes the magnetic order to higher values of $J_\perp$. Our results provide valuable insights into the complex nature of competing interactions within the Kondo-Hubbard model, contributing to the understanding of quantum phase transitions of Kondo lattice model.

Abbreviations

RKKY	Ruderman-Kittel-Kasuya-Yosida
VCA	Variational Cluster Approximation

CPT	Cluster Perturbation Theory
AFM	Antiferromagnetism

Acknowledgments

We gratefully acknowledge conversations with D. Sénéchal. Computing resources were provided by Compute Canada and Calcul Québec.

Authors Contributions

All the authors contributed to the article during all the processes.

Conflicts of Interest

The authors declare no conflicts of interest.

References

[1] K. Andres, J. E. Graebner, and H. R. Ott, "$4f$-virtual-bound-state formation in $\mathrm{ceal_3}$ at low temperatures," *Phys. Rev. Lett.*, vol. 35, pp. 1779–1782, Dec 1975

[2] F. Steglich, J. Aarts, C. D. Bredl, W. Lieke, D. Meschede, W. Franz, and H. Schäfer, "Superconductivity in the presence of strong pauli paramagnetism: $\mathrm{Cecu_2si_2}$," *Phys. Rev. Lett.*, vol. 43, pp. 1892–1896, Dec 1979.

[3] E. Bucher, J. P. Maita, G. W. Hull, R. C. Fulton, and A. S. Cooper, "Electronic properties of beryllides of the rare earth and some actinides," *Phys. Rev. B*, vol. 11, pp. 440–449, Jan 1975.

[4] G. R. Stewart, "Non-fermi-liquid behavior in d- and f-electron metals," *Rev. Mod. Phys.*, vol. 73, pp. 797–855, Oct 2001.

[5] J. Kondo, "Resistance Minimum in Dilute Magnetic Alloys," *Progress of Theoretical Physics*, vol. 32, pp. 37–49, 07 1964.

[6] M. Amundsen, A. Brataas, and J. Linder, "Rkky interaction in rashba altermagnets," *Phys. Rev. B*, vol. 110, p. 054427, Aug 2024.

[7] J. P. L. Faye, M. N. Kiselev, P. Ram, B. Kumar, and D. Sénéchal, "Phase diagram of the hubbard-kondo lattice model from the variational cluster approximation," *Phys. Rev. B*, vol. 97, p. 235151, Jun 2018.

[8] O. Ndiaye, D. Dione, A. Traoré, A. S. Ndao, and J. P. L. Faye, "Spiral magnetism and chiral superconductivity in a kondo-hubbard triangular lattice model," *Phys. Rev. B*, vol. 105, p. 045116, Jan 2022.

[9] V. N. Kotov, B. Uchoa, V. M. Pereira, F. Guinea, and A. H. Castro Neto, "Electron-electron interactions in graphene: Current status and perspectives," *Rev. Mod. Phys.*, vol. 84, pp. 1067–1125, Jul 2012.

[10] P. Vogt, P. De Padova, C. Quaresima, J. Avila, E. Frantzeskakis, M. C. Asensio, A. Resta, B. Ealet, and G. Le Lay, "Silicene: Compelling experimental evidence for graphenelike two-dimensional silicon," *Phys. Rev. Lett.*, vol. 108, p. 155501, Apr 2012.

[11] F. F. Assaad and I. F. Herbut, "Pinning the order: The nature of quantum criticality in the hubbard model on honeycomb lattice," *Phys. Rev. X*, vol. 3, p. 031010, Aug 2013.

[12] S. Raghu, X.-L. Qi, C. Honerkamp, and S.-C. Zhang, "Topological mott insulators," *Phys. Rev. Lett.*, vol. 100, p. 156401, Apr 2008.

[13] J.-H. Chen, L. Li, W. G. Cullen, E. D. Williams, and M. S. Fuhrer, "Tunable kondo effect in graphene with defects," *Nature Physics*, vol. 7, p. 535, Apr 2011.

[14] T. O. Wehling, A. V. Balatsky, M. I. Katsnelson, A. I. Lichtenstein, and A. Rosch, "Orbitally controlled kondo effect of co adatoms on graphene," *Phys. Rev. B*, vol. 81, p. 115427, Mar 2010.

[15] H. C. Kandpal and J. van den Brink, "Calculation of magnetic exchange couplings in the $s = 3/2$ honeycomb system $(\mathrm{bi_3mn_4o_{12}})\mathrm{no_3}$ from first principles," *Phys. Rev. B*, vol. 83, p. 140412, Apr 2011.

[16] I. Bloch, J. Dalibard, and W. Zwerger, "Many-body physics with ultracold gases," *Rev. Mod. Phys.*, vol. 80, pp. 885–964, Jul 2008.

[17] C. Dahnken, M. Aichhorn, W. Hanke, E. Arrigoni, and M. Potthoff, "Variational cluster approach to spontaneous symmetry breaking: The itinerant antiferromagnet in two dimensions," *Phys. Rev. B*, vol. 70, p. 245110, Dec 2004.

[18] D. Sénéchal, D. Perez, and D. Plouffe, "Cluster perturbation theory for hubbard models," *Phys. Rev. B*, vol. 66, p. 075129, Aug 2002.

[19] M. Potthoff, M. Aichhorn, and C. Dahnken, "Variational cluster approach to correlated electron systems in low dimensions," *Phys. Rev. Lett.*, vol. 91, p. 206402, Nov 2003.

[20] D. Sénéchal, P.-L. Lavertu, M.-A. Marois, and A.-M. S. Tremblay, "Competition between antiferromagnetism and superconductivity in high-T_c cuprates," *Phys. Rev. Lett.*, vol. 94, p. 156404, Apr 2005.